PHYSICAL REVIEW B VOLUME 16, NUMBER 12 15 DECEMBER 1977

Phonon spectroscopy. I. Spectral distribution of a phonon pulse*

W. E. Bron and W. Grill
Department of Physics, Indiana University, Bloomington, Indiana 47401
(Received 9 June 1977)

A vibronic-sideband spectrometer has been developed capable of resolving the spectral, spatial, and temporal evolution of a phonon distribution propagating in a solid. As a first application of the spectrometer, a determination has been achieved of the spectral distribution of a phonon pulse which has been generated by Joule heating in a metal film and which has crossed an interface between the film and a crystalline solid. The spectral distribution observed at low electrical input power agrees with existing theory, but the agreement becomes progressively worse as the input power exceeds 12 W/mm^2. In order to account for the experimental results an empirical frequency-dependent filtering action is defined, which hinders the transport into the crystal of phonons with frequencies above 1 THz. It is shown that a more complete treatment of the phonon transport would have to assay the effects in the heater film of umklapp processes, of the breakdown of the deformation-potential model of electron-phonon coupling, of phonon decay, and the effect of the frequency dependence of interface mismatch. The phonon spectrometer has a wider applicability than demonstrated in this paper and in the paper immediately following. The main characteristics, and limitations, of the spectrometer are discussed in some detail.

I. INTRODUCTION

A phonon spectrometer has been developed capable of resolving the spectral, spatial, and temporal distribution of phonons propagating in a solid. The spectrometer uses as the detecting element the vibronic sidebands associated with certain luminescent transitions at probe ions placed in dilute concentration in the solid. As a first application of the spectrometer we determine the spectral distribution of phonons which are generated in a constantan thin film through Joule heating, and which cross an interface between the thin film and the solid which is a crystal of SrF_2 containing Eu^{2+} ions.

The application of metal "heater" films to the study of the phonon transport properties of solids has received wide attention since the early work of von Gutfeld and Nethercot.[1] It has usually been assumed that the phonons which are injected across the film-crystal interface follow a Bose-Einstein distribution. According to the generally accepted acoustic mismatch (AM) model,[2,3] the temperature associated with the distribution can be obtained through an energy balance between the electrical power into the heater film and the transmission of phonons across the interface.

The acoustic mismatch model has rarely been challenged. Two major exceptions are the papers by Maris[4] and those of Perrin and Budd.[5] These authors note that the electron-phonon interaction strength in the metal increases with phonon frequency, i.e., the interaction generates high-frequency phonons more efficiently than low-frequency phonons. Therefore, and depending on the interface characteristics,[4] a phonon distribution which differs from a Bose-Einstein distribution should be generated in the film.

In the AM and Perrin-Budd (PB) models it is tacitly assumed that the transport through the interface is frequency independent and determinable from acoustic-mismatch theory, i.e., from simple continuum mechanics. The assumption, which may well be applicable in the long-wavelength regime, should be expected to break down when the phonon wavelength approaches the dimension of interatomic distances. Indeed, under conditions in which the phonon distribution contains primarily phonons of frequency less than 1 THz (low heater power,[6] or low frequency excitation[7]), the AM model has been demonstrated to adequately describe experimental results. In contrast, it has been demonstrated that experimental results from heater films pulsed to higher powers, hence with higher phonon frequencies, do not agree with theory.[8] Yet it is precisely in the high-frequency phonon regime in which such interesting phenomena as phonon-phonon interactions, phonon-impurity, and phonon-imperfection scattering become strong, and in which a critical comparison between the AM and PB model can be most readily made.

In the present experiment we measure directly the frequency distribution of phonons which are generated in a heater film and are transmitted across a film-crystal interface. We find indeed that the models are applicable only at low power levels, and that at high phonon frequencies an unidentified additional process hinders phonon transmission across the interface.

In an experiment described in the paper immediately following[9] we apply the vibronic sideband

spectrometer to determine the spectral, spatial, and temporal evolution of the phonon pulse after it has crossed the interface and is propagating inside the solid.

II. EXPERIMENTAL METHODS

The primary experimental observation is the luminescence associated with the $4f^6 5d(\Gamma_8) \rightarrow 4f^7(^8S_{7/2})$ electronic transition of the Eu^{2+} ion in a SrF_2 crystal. The crystal, obtained from Optovac, Inc.,[10] nominally contains 0.1 mole% of Eu^{2+} and is roughly rectangular in shape with approximately 7×7 mm cross section and about 1 cm length. The faces have been carefully polished with diamond grit down to 0.25 μm in size. During the experiment all but one face of the crystal is in vacuum of less than 10^{-8} Torr. The remaining face is attached with epoxy on to a thin wall cylinder which forms the bottom of the helium reservoir of an optical Dewar. The ambient temperature of the crystal is nominally 4.2 °K. A 50-Ω constantan film approximately 3000-Å thick which is evaporated onto a (100) end surface of the crystal after the crystal has been very carefully cleaned and brought to a vacuum of 10^{-6} Torr prior to evaporation. The film-crystal interface has the dimension of 5×0.2 mm. Films deposited in this manner can be pulsed up to 800 V (12.8 kW) for periods of 20 nsec after the crystal is brought to near 1 °K.

Luminescence is excited with a N_2 laser having a 10-nsec pulse duration and 20 w average pulse power. The laser beam is focused inside the crystal to a focal column approximately 0.1 mm in diameter, the column being parallel to the long dimension of the heater film. The luminescent column is collected and focused on to the entrance slit of a tandem 1- and 0.25-m Czerny-Turner grating spectrometer. Figure 1 is a schematic illustration of the optical arrangement. The beam splitter and photodiode shown just inside the spectrometer slit are used to monitor the integrated luminescence which varies some 10% from pulse to pulse due to the variation in the output of the N_2 laser. A second photodiode attached to one of the Dewar windows is used to monitor the onset of the luminescence. The location of the luminescent column in the crystal can be visually determined using a telescope with a calibrated vernier eyepiece.

Under actual experimental conditions the 50-Ω constantan film is pulsed in a range from 25 to 500 V for 20–200 nsec, depending on the voltage. The voltage across the constantan film is obtained by determining to within ±2% the net of the voltage pulse incident on the heater, the reflected pulse, if any, and the losses through the 50-Ω coaxial connecting cables. The laser is pulsed at twice the repetition rate of the heater pulse, such that every other luminescent pulse is in the presence of an injected phonon distribution.

The luminescence from the Eu^{2+} ion transition has a lifetime of the order of 1 μsec. Only a gated portion of 200 nsec is used as the signal. The onset of the gate is delayed by 200 nsec after the onset of the laser pulse, but is set to coincide with the onset of the heater pulse. As will be demonstrated in the following paper[9] it is important to limit the gate time to no more than 200 nsec after the heater pulse if changes in the phonon spectral distribution due to phonon decay are to be avoided. In the spectral region of the $4f^6 5d(\Gamma_8)$ emitting state of Eu^{2+}, there also exist the A_1 and A_2 levels of the Jahn-Teller multiplet.[11] We attribute the additional observed luminescence, shifted relatively to the zero-phonon line by -0.65 and -10.15 Å, respectively, to these lines. The additional luminescence dies out in periods of 50 nsec and less than 20 nsec, respectively. This complication is removed by delaying the onset of the gate by 200 nsec relative to the laser pulse. The gated signal from the photomultiplier (PMT)

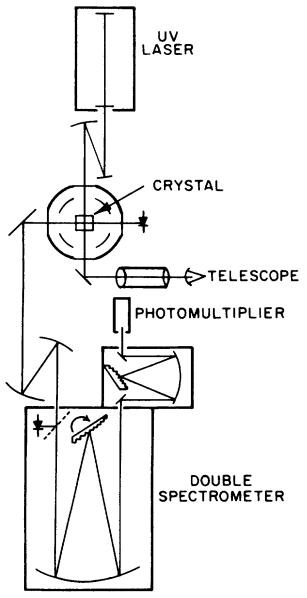

FIG. 1. Optical arrangement. The crystal is in vacuum and attached on one face directly to the bottom of a liquid helium vessel. The pump light from the uv laser actually enters the optical dewar from a bottom window such that the luminescent column is parallel to the input slit of the spectrometer. The roles of the photodiodes and telescope are discussed in the text.

is electronically divided on a pulse to pulse basis for the variation in the N_2-laser output and displayed as a function of spectral frequency as the "direct" signal. Simultaneously, a "difference" signal is obtained by sending the corrected gated PMT output through a lock-in amplifier tuned to the repetition frequency of the phonon pulses. The difference signal contains the incremental luminescence due solely to the presence of the injected phonon distribution. This procedure eliminates all effects due to the ambient concentration of phonons, and all linear effects arising from the phonons generated at the Eu^{2+} ions by nonradiative decay from the state excited by absorption of the laser light to the $4f^5 5d(\Gamma_8)$ emitting state. In order to check the possible effect of any nonlinear interaction of the nonradiatively produced phonons and the injected phonons, if any, the N_2 laser intensity was reduced by one-half. No change is observed in the spectral distribution of the difference signal.

In the experiment described in this paper the luminescent column is repetitively linearly swept by mechanical means, over an integrating volume bounded by the heater and by surfaces which are ≥ 1 mm away from the heater in any direction, and such that over the gate time the incremental luminescence from all phonons crossing the film-crystal interface is detected equally regardless of the phonon propagation velocity.

A typical direct (dashed line) and difference (solid line) signal is displayed in Fig. 2. The frequencies of the phonon sidebands are given relative to the center of the so-called "zero-phonon" line which appears at 4.2 °K at 4011 Å. The optical

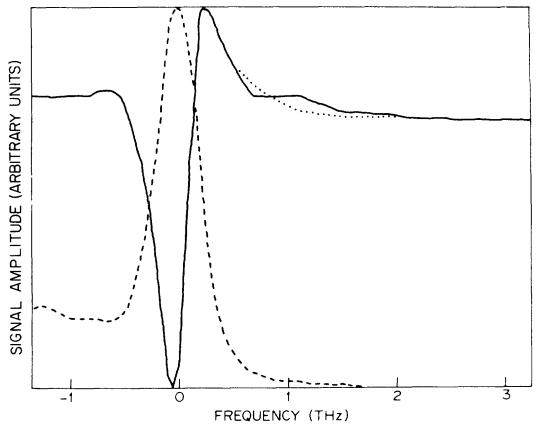

FIG. 2. Direct and differential signal amplitude as a function of frequency measured relative to the frequency of the zero-phonon line (---- direct signal, ——— difference signal). The dotted section is that expected from a thermalized phonon distribution.

spectrometer slit was normally set to 100 μm which corresponds to a spectral resolution of 0.8 Å. In Fig. 2 only a small portion of the Stokes sideband (low-frequency side of the zero-phonon line) is displayed. In the direct signal a change in the intensity of the anti-Stokes sideband (high-frequency side of the zero-phonon line) is observed only under the highest heater-pulse power. In the absence of any heater pulse the difference signal is, of course, zero for all frequencies. In the presence of the injected phonon pulses a signal is observed of the form illustrated in the solid line. The zero in the amplitude of this signal has been offset from that of the direct signal by an amount equal to that indicated at +3 THz. An increase in the anti-Stokes differential signal can be clearly observed. The strength of this signal depends on the input power. Under present experimental conditions anti-Stokes sidebands from input powers of ≥ 12 W/mm^2 can be detected. In the region of the zero-phonon line, an apparent derivative signal is observed which arises primarily from two sources. High-order interaction between the phonons and the bound electrons of the Eu^{2+} ions lead to a frequency shift and broadening of the zero-phonon line. In addition, any incremental oscillator strength in the sideband is subtracted from that of the zero-phonon line. The origin of these effects has been known for some time[12] and will not be discussed further here. The first derivative component of the signal can be numerically subtracted out to some extent[13] by noting that the difference signal must vanish at the center of the zero-phonon line and that the only nonsymmetric component comes from a shift in the line. However, it is only for frequencies of ≥ 0.2 THz that uncertainties in the numerical subtraction process become less than those of the experimental data. The spectral resolution of the phonon spectrometer is accordingly limited to frequencies greater than 0.2 THz and extends to the phonon cutoff of the crystal. Anti-Stokes difference signals have been observed to greater than 6 THz. The Stokes difference sideband carries the same information as the anti-Stokes sideband but at lower signal-to-noise levels. The Stokes difference signal has not, accordingly, been analyzed in detail here.

Finally, as is indicated in Sec. III A, it is necessary to determine in detail the Stokes direct signal at very low temperature and in the absence of any injected phonon pulse. This has been carried out with the sample at $T \sim 1$ °K. The results, corrected for the multiphonon background,[14,15] is displayed in Fig. 3. In the analysis of the anti-Stokes difference signal only the portion $0 < \nu < 5$ THz is actually used.

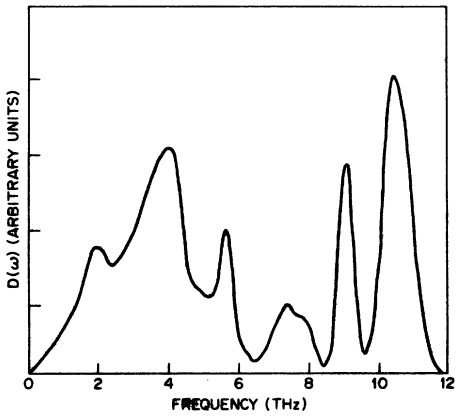

FIG. 3. One-phonon Stokes vibronic sideband obtained with the sample at ~1 °K and no injected phonon pulses. The multiphonon background has been subtracted out.

III. THEORETICAL BACKGROUND

A. Vibronic sidebands

Vibronic sidebands arise from the interaction between the time-varying crystal field associated with phonons and an electronic transition localized at probe ions in the crystal. The unperturbed electronic transition gives rise to a "zero phonon" spectral line. The sidebands represent the simultaneous absorption and emission of one or more phonons during the transition. The application of vibronic spectra to determine phonon distributions has been demonstrated many times. (See, e.g., Ref. 16 and references cited therein. For general reviews of the topic see Ref. 17.)

The Stokes sideband, in the presence of ambient phonons plus an injected phonon pulse, involves the emission of phonons. The intensity of the sideband at a phonon frequency ω can be written as

$$I_S(\omega) = \frac{e^2\hbar}{4\omega}[n(\omega)+1]\sum_{\Gamma} F(\Gamma)\rho(\omega,\Gamma)F'(\Gamma), \quad (1a)$$

whereas, the intensity of the anti-Stokes sideband, which involves the absorption of phonons, is written as

$$I_{AS}(\omega) = \frac{e^2\hbar}{4\omega}n(\omega)\sum_{\Gamma} F(\Gamma)\rho(\omega,\Gamma)F'(\Gamma). \quad (1b)$$

In Eqs. (1a) and (1b), $n(\omega)$ is the phonon distribution functions, $\rho(\omega,\Gamma)$ is the phonon density of states projected on to the irreducible representations, Γ, which are consistent with the electronic transition, $F(\Gamma)$ is the electron-phonon interaction operator. The corresponding differential intensity $\Delta I(\omega)$ follows from Eqs. (1a) and (1b) by subtraction of the contribution of the ambient phonon distribution.

It should be noted that in the expression (1a) $n(\omega)$ vanishes at low temperatures and no injected phonon pulse, and that only the sum on Γ (times $e^2\hbar/4\omega$) survives. We refer to the surviving part as the detectivity function $D(\omega)$. It has been repeatedly demonstrated that $D(\omega)$ can be calculated directly from shell-model representations of the lattice dynamics and, in the case of ionic solids, from a Coulombic electron-phonon interaction. The method has, in fact, been shown to work in considerable detail in a number of crystal systems, including the one used in the present work, i.e., $SrF_2:Eu^{2+}$.[14,18]

For the present purposes it is not necessary to carry out detailed calculations of $D(\omega)$. It is obvious that the summation over Γ can be eliminated by dividing Eq. (1b) by the experimentally obtained $D(\omega)$. The result is

$$\Delta I_{AS}(\omega)/D(\omega) = \Delta n(\omega). \quad (2)$$

The primary information which is, accordingly, extracted from the experimental data is the differential distribution function $\Delta n(\omega)$ of the phonon pulse.

B. Acoustic mismatch model

In the acoustic mismatch model (AM) it is assumed that the electrons and phonons in the metal heater film reach the same temperature T in a time short (of order 10^{-10} sec) compared to the length of the voltage pulse. The temperature T reached by the metal film is determined from an energy balance between the electrical power into the film and the thermal radiation from the film into the crystal. It will be convenient to refer to the electron temperature as T_e and the phonon temperature as T_p. The film-crystal interface is usually described by a frequency-independent transmission coefficient determined from continuum mechanics.

The spectral energy flux transmitted from the heater across an interface of area A into a large crystal at temperature T_c is then

$$\frac{P(\omega,T_p,T_c)}{A} = \frac{\hbar\omega^3}{8\pi^2}\frac{e_l}{C_l^h(\omega)^2}[n_{BE}(\omega,T_p)-n_{BE}(\omega,T_c)] + \frac{\hbar\omega^3}{4\pi^2}\frac{e_t}{C_t^h(\omega)^2} \times [n_{BE}(\omega,T_p)-n_{BE}(\omega,T_c)]. \quad (3)$$

In Eq. (3), the superscript h refers to the heater film, which is treated as a Debye solid, and e_l, e_t are the frequency-independent interface transmission coefficients for longitudinally and transversely polarized phonons, respectively. $C_l^h(\omega)$, $C_t^h(\omega)$ are the corresponding frequency-dependent

phase velocities of the phonons in the metal film, and $n_{BE}(\omega, T)$ is the Bose-Einstein (BE) distribution function evaluated at the appropriate temperature. The two transversely polarized phonon branches are assumed to be degenerate.

The temperature T_p is found by equating the integral of the spectral energy flux over all phonon frequencies to the total electric power into the heater film. Since Eq. (3) must be evaluated up to values of nearly one-third the Debye temperature it will be necessary to include the frequency dependence of the phase velocities. Since the full dynamical properties of constantan are not readily attainable in analytical form, we follow the approximations proposed by Weis.[3] In the Debye solid representing the constantan film all phonons have the same maximum wave vector $|q_{max}|$, but the longitudinal and transverse branches have different maximum frequencies, ω_{max}. From the density of states in q space, and the concentration of atoms in the solid N/V, it follows that

$$q_{max} = (6\pi^2 N/V)^{1/3} . \tag{4}$$

Moreover, we follow Weis[3] and take the dispersion of constantan to be

$$\omega(q, \sigma) = C_\sigma^h(\omega = 0) \frac{2|q_{max}|}{\pi} \sin\left(\frac{\pi |q|}{2|q_{max}|}\right) , \tag{5}$$

where σ is the polarization branch index ($\sigma = l$ for the longitudinal branch, and t for the transverse branches). Equations (4) and (5) define ω_{max} and the phase velocities $C_\sigma^h(\omega) = \omega(q, \sigma)/q$.

Formally, the total energy flux across the interface becomes

$$\frac{P(T_p, T_c)}{A} = \frac{\hbar e_l}{8\pi^2} \int_0^{\omega_{max}^l} d\omega \frac{\omega^3}{C_l^h(\omega)^2} [n_{BE}(T_p) - n_{BE}(T_c)] + \frac{\hbar e_t}{4\pi^2} \int_0^{\omega_{max}^t} d\omega \frac{\omega^3}{C_t^h(\omega)^2} [n_{BE}(T_p) - n_{BE}(T_c)] . \tag{6}$$

C. Perrin-Budd model

The model introduced by Perrin and Budd[5] (PB) differs from the AM model in that an attempt is made to include in a rather simplified way the frequency dependence of the electron-phonon interaction in the metal film. In this model the excited electron gas is assumed to thermalize rapidly reaching thereby a temperature T_e. Two coupled rate equations describe the change in the number of phonons as they are driven by the excited electron gas and are lost through transport across the film-crystal interface.

The increase with time in the number of phonons with wave vector $\vec{q}$ and polarization branch index σ, due to the electron-phonon interaction is

$$\left(\frac{dN(\vec{q}, \sigma)}{dt}\right)_{ep} = \frac{\bar{N}(\vec{q}, \sigma, T_e) - N(\vec{q}, \sigma)}{\tau_{ep}} , \tag{7a}$$

whereas the net loss of phonons across the interface is

$$\left(\frac{dN(\vec{q}, \sigma)}{dt}\right)_{b} = \frac{\bar{N}(\vec{q}, \sigma, T_c) - N(\vec{q}, \sigma)}{\tau_b} . \tag{7b}$$

In Eqs. (7a) and (7b), $\bar{N}$ is the phonon number obtained from the Bose-Einstein distribution function, evaluated at $\vec{q}, \sigma$ and the appropriate temperatures. The parameter τ_b is the time required for a phonon of $\vec{q}, \sigma$ to relax toward the crystal temperature T_c. Perrin and Budd take this quantity to be independent of phonon frequency. In order to have the PB model be consistent with relations (4) and (5) above, we take at this point the identification of τ_b one step further by writing it as

$$\tau_b = 4\eta_\sigma d / C_g(q, \sigma) , \tag{8}$$

in which η_σ is a frequency-independent reflection factor which we take to be to e_σ^{-1},[19] d is the thickness of the film, and C_g is the frequency dependent group velocity of a phonon of q, σ obtained by differentiating Eq. (5) with respect to q.

The explicit frequency dependence of the electron-phonon interaction time is taken to follow that of the Pippard model,[20] i.e.,

$$\tau_{ep}(q, \sigma) = [6\rho C_\sigma(\omega = 0)/\pi n m v_F] \, 1/\omega(q, \sigma) , \tag{9}$$

in which ρ is the mass density of the heater metal, n is the electron density, m the electron mass, and v_F the Fermi velocity. In an isotropic solid the interaction potential only couples longitudinally polarized phonons to the electrons. This is not the case in anisotropic materials for which the form of the coupling to transversely polarized phonons is analogous to that of Eq. (9).[21]

For typical metals the time for the system to reach a steady state is shown by Perrin and Budd to be of the order of a nanosecond, i.e., times short compared to the time resolution of experimental observations. It is necessary, therefore, to consider Eqs. (7a) and (7b) only in the steady-state limit in which

$$N(\vec{q}, \sigma) = [\tau_b \bar{N}(\vec{q}, \sigma, T_e) + \tau_{ep} \bar{N}(\vec{q}, \sigma, T_c)]/(\tau_{ep} + \tau_b) . \tag{10}$$

Equation (5) is again used to transform, from q space to ω space, the expression for the spectral energy flux across the film-crystal interface, which in the PB model becomes

$$\frac{P(\omega, T_e, T_c)}{A} = \frac{\hbar\omega^3}{8\pi^2} \frac{e_l}{C_l^h(\omega)^2} [n_{PB}(\omega) - n_{BE}(\omega, T_c)] + \frac{\hbar\omega^3}{4\pi^2} \frac{e_t}{C_t^h(\omega)^2} [n_{PB}(\omega) - n_{BE}(\omega, T_c)] . \tag{11}$$

In Eq. (11), $n_{PB}(\omega)$ is the Perrin-Budd phonon distribution function in ω space obtained from $N(q,\sigma)$ by summing in the usual way over q space and assuming a Debye density of states. It is clear from Eq. (10) that n_{PB} does not resemble a Bose-Einstein distribution, i.e., no temperature can be assigned to the distribution.

In steady state the electron temperature T_e can be determined from an energy balance between the total electrical power into the metal film and the loss of power from the electron gas to the phonons. The result is[22]

$$P_T(T_e,T_c)=\int_0^{\omega_{\max}^l}\int_0^{\omega_{\max}^t} d\omega\,\frac{\hbar\omega}{\tau_{ep}+\tau_b}\,\frac{\omega^2}{C_\sigma^h(\omega)^3}\times[n_{BE}(\omega,T_e)-n_{BE}(\omega,T_c)]\,. \tag{12}$$

It should especially be noted that we have chosen to use for the description of the phonon transport across the film-crystal interface the parameters which appear in the original forms of the AM[2] and the PB[5] models; i.e., the interface transmission coefficients e_σ and τ_b, respectively. These parameters do not necessarily yield equivalent interface properties. It should accordingly be expected that, for the same input power, T_e differs for the two models. Consequently, the models should *not* be compared at the same temperature. On the other hand, a physically meaningful comparison between the two models and to the experimental results can be made through a normalization to the total electrical input power, i.e., on the basis of Eqs. (6) and (12). This comparison will be made in Sec. IV.

D. Maris criterion

Before proceeding to the experimental results it is necessary to consider a criterion set forth by Maris[4] under which one might expect the phonon distribution in the heater film to reach a Bose-Einstein distribution. It is clear that if the heater film is removed from the crystal, and isolated in a vacuum, that any phonon distribution in the film will in time reach an equilibrium thermal distribution with $T_p=T_e$. A less severe criterion may be formulated for a heater film deposited on a crystal in which it is simple required that the rate of escape of phonons of all frequencies from the film to the crystal be considerably less than the rate at which they are generated by the electron-phonon interaction. Maris has shown that the latter criterion can be expressed as

$$e_\sigma \ll \frac{4d}{\tau_{ep}C_q(q,\sigma)} \equiv \frac{4d}{\lambda_{ep}(q,\sigma)} \equiv E_{q,\sigma}\,, \tag{13}$$

in which $\lambda_{ep}(q,\sigma)$ is an effective electron-phonon interaction length for phonons of q,σ. Maris has tabulated λ_{ep} for several metal films including constantan. For the range of frequencies of interest here, i.e., $0.2<\nu<5$ THz, and for $d=3\times10^3$ Å one obtains $0.3\le E_{q,\sigma}\le 7.5$, respectively. Values of the transmission coefficients e_l and e_t of 0.82 and 0.76, respectively, are obtained as twice the corresponding Γ_l,Γ_t displayed in Figs. 4 and 5 of Ref. 2. Accordingly, in the present experiment, the criterion (13) is not fulfilled for low-frequency phonons. We find, therefore, that both the PB model and the Maris criterion predict that the phonons crossing the film-crystal interface will not follow a Bose-Einstein distribution.

IV. EXPERIMENTAL RESULTS AND COMPARISON TO THEORY

The anti-Stokes difference sideband has been obtained as described in Sec. II for input powers of 12.5, 200, 800, and 5000 W/mm^2. In accordance with Eq. (2), the sideband for frequencies ≥ 0.2 THz is then divided by $D(\omega)$ to yield $\Delta n(\omega)$. The result is displayed in Fig. 4.

It should be noted that the general form of $\Delta n(\omega)$ follows that expected from the Bose-Einstein distribution, except for the marked feature near 0.6 THz which is always observed but for which we have no explanation. Except for this feature, it would, in fact, be possible to force a fit to a BE distribution and obtain a "temperature" for $\Delta n(\omega)$. To within a multiplicable factor each

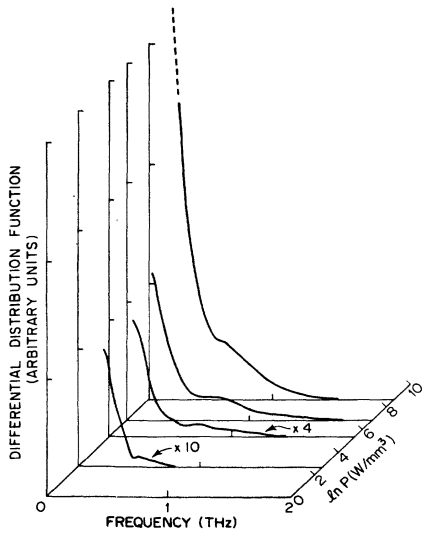

FIG. 4. Differential distribution function $\Delta n(\omega)$ as a function of frequency at a number of different input powers (P). Note that the functions for the lowest two input powers have been increased by factors of 4 and 10.

TABLE I. Comparison of model temperatures.

Input power (W/mm^2)	12.5	2×10^2	5×10^3
PB: T_e (°K)	14.0	26.3	62.0
AM: $T_e=T_p$ (°K)	12.0	23.5	57.0

$\Delta n(\omega)$, regardless of the input power, can be fit to a distribution at $T=13$ °K. As is shown in Table I, with the exception of the lowest input power, $T=13$ °K is below that of the AM temperature T_p and the PB temperature T_e obtained from Eqs. (6) and (12).

As noted in Sec. III C, a physically significant comparison between the data and the two models should, in any event, not be made on the basis of temperatures but rather in terms of the spectral energy flux normalized to the total input power. For this purpose the following procedure was adopted to normalize the experimental data to the input power. Since $\Delta n(\omega)$ can be extracted from the data only over the frequency range $0.2<\nu<\sim3$ THz [above ~3 THz the uncertainty in $\Delta n(\omega)$ due to numerical manipulation of the data is of the same magnitude as $\Delta n(\omega)$], a 13 °K BE distribution, properly scaled to the data, is used to extend the data below 0.2 THz and between ~3–5 THz. This procedure is justified because of the general shape of $\Delta n(\omega)$ as noted above, and because the spectral energy flux is at least an order of magnitude smaller in these regions than in the main region of the distribution. The experimental results, of course, involve the spectral energy flux crossing the interface as measured inside the SrF_2 crystal. To determine this quantity we use directly the density of phonon states, $\rho(\nu)$ of SrF_2 as has been determined from neutron scattering data.[23] The experimental spectral energy flux

TABLE II. Model parameters.

Parameter	Units	Constantan	SrF_2
e_l		0.82 [a]	
e_t		0.74 [a]	
$C_l(\omega=0)$	km sec^{-1}	5.24 [b]	5.46 [c]
$C_t(\omega=0)$	km sec^{-1}	2.64 [b]	2.80 [c]
q_{max}	m^{-1}	1.72×10^{10}	1.349×10^{10}
ν^l_{max}	THz	9.14 [b]	7.17
ν^t_{max}	THz	4.60 [b]	3.61
ρ	g cm^{-3}	8.80 [b]	4.32

[a] e_σ equals twice the Γ_σ found in Ref. 2.
[b] Reference 8.
[c] Reference 24.

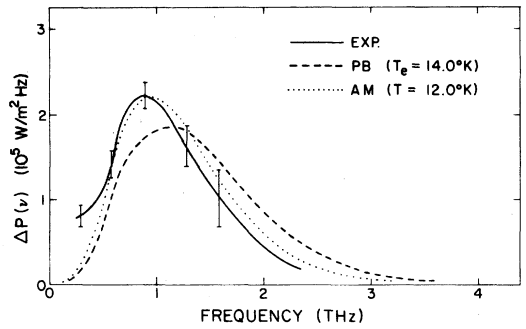

FIG. 5. Comparison of the experimentally determined differential spectral energy flux to those obtained from the AM and PB models. Each function has been normalized to the input power of 12.5 W/mm^2. In this figure, and in Figs. 6 and 7, the vertical bars are representative of the uncertainty in $\Delta P(\nu)$ in the frequency region in which they are drawn. The actual curve for the experimental $\Delta P(\nu)$ is determined over its entire range with points spaced 0.02 THz apart.

ΔP_{exp} is defined as the product $h\nu\rho(\nu)\Delta n(\nu)$, in which the experimental distribution, $\Delta n(\nu)$ is normalized such that the integration of ΔP_{exp} over ν is equal to the input power; i.e., in a manner equivalent to Eqs. (6) and (12). Table II is a compilation of the various model parameters.

The resultant comparison is presented in Figs. 5–7 for three input powers. The ordinate is labeled as the differential spectral energy flux $\Delta P(\nu)$ as a reminder that only the incremental spectral energy flux due to the injected phonons is displayed. The secondary peak in ΔP_{exp} observable in Figs. 6 and 7 near 2.5 THz is a direct consequence of the use of the density of states of SrF_2, obtained from neutron scattering, in the calculation of ΔP_{exp} from Δn_{exp}. The secondary peak does not appear if a Debye density of states is

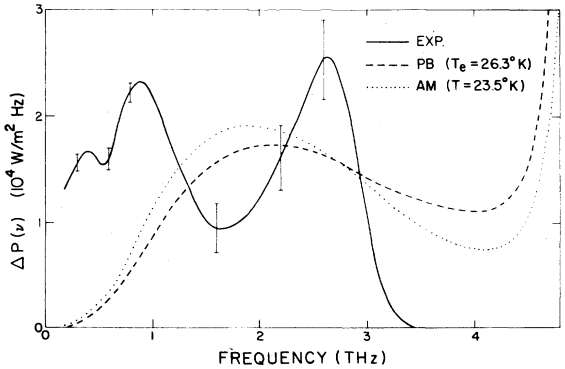

FIG. 6. Comparison of the experimentally determined differential spectral energy flux to those obtained from the AM and PB models. Each function has been normalized to the input power of 2×10^2 W/mm^2.

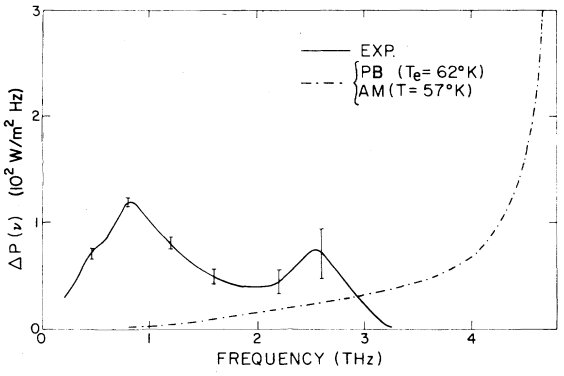

FIG. 7. Comparison of the experimentally determined differential spectral energy flux to those obtained from the AM and PB models. Each function has been normalized to the input power of 5×10^3 W/mm^2.

assumed for SrF_2.

The result shown in Fig. 5 is consistent with the previous observations by others[6,7] that qualitative agreement exists between experiment and the AM model at low phonon frequencies and low input powers. Moreover, in this regime the experimental results are now seen to be in rough agreement with the PB model. We conclude, however, from the results illustrated in Figs. 6 and 7 that the agreement progressively deteriorates as the power in the phonon pulse, and hence the relative flux of high-frequency phonons, increases. Also note that the shape of the experimentally observed differential spectral energy function ΔP_{exp} does not vary much over the range of input powers. It is primarily the amplitude of the function which changes with input power.

V. DISCUSSION

A. Assumptions of the models

As a first step in an analysis of the results we discuss some of the inherent assumptions in the AM and PB models in order to determine whether any of these may account for the observed discrepancy between experiment and theory. The basic simplifying assumptions in both models is that the heater film can be adequately described as an isotropic Debye solid with a spherical energy surface, that umklapp processes can be neglected, as can the anisotropy in the electron distribution caused by the current flow, and that the electron-electron scattering time is short compared to experimental times such that the electron gas reaches a Fermi-Dirac distribution given by a temperature T_e. Inherent implicitly in the AM model, and explicitly in the PB model, is the assumption that the electron and the phonon transport through the film can be described by simple rate processes, that transport through concentration gradients can be neglected, and that the characteristic escape time for phonons from the heater film depends only on the film thickness and the phonon group velocity. Perhaps the most serious of all is the usual additional simplifying assumption, made in evaluating both models, that the transmission probability across the film-crystal interface is independent of phonon frequency and obtainable from acoustic mismatch theory. The only proviso for high-frequency phonon transport is that the cutoff frequency for phonons in the transport medium be equal or greater than that in the film. To these assumptions we have added those by Weis[3]; namely, that the dispersion relationship, and hence the phonon group velocities, can be obtained from Eq. (5).

It is clear that a detailed critique of the validity of all these assumptions is outside the scope of this paper. A few general remarks can, however, be made. The constantan heater is polycrystalline so that at least in a macroscopic sense the film is isotropic. In a microscopically isotropic crystal the Pippard mechanism[20] does not permit coupling to transversely polarized phonons. Constantan certainly is microscopically anisotropic and transversely polarized phonons have indeed been observed in experiments using constantan heater films on other substrates[1] and on SrF_2:Eu^{2+}.[25] However, the general properties of these phonons, including their frequency distribution, is not expected to differ much from those of the longitudinal phonons.[21]

In order to discuss the possible effect of umklapp processes we rely on the published dispersion curves of[26] Cu and Ni,[27] and the spectral energy flux obtained for constantan from the AM and PB models. The spectral energy flux as a function of temperature as determined from the AM model (with dispersion of a linear chain) has been published by Weis.[3] We present in Fig. 8 the analogous spectral energy flux obtained from the PB model at various temperatures, T_e. Weis[8] has also tabulated the Debye cutoff frequency for constantan, copper, and nickel and shows that ν_{max} for constantan for each polarization branch lies roughly halfway between the values for Cu and Ni. Based on this comparison the frequency of transversely polarized phonons in constantan which have q nearly halfway to the Brillouin zone boundary is estimated to be about 3.4 THz. Above this frequency range, multiphonon and finally direct umklapp processes can be expected to occur. From the calculations of the spectral energy flux at various temperatures it can be seen that for $T_e > 16$ °K a large fraction of the total phonon power

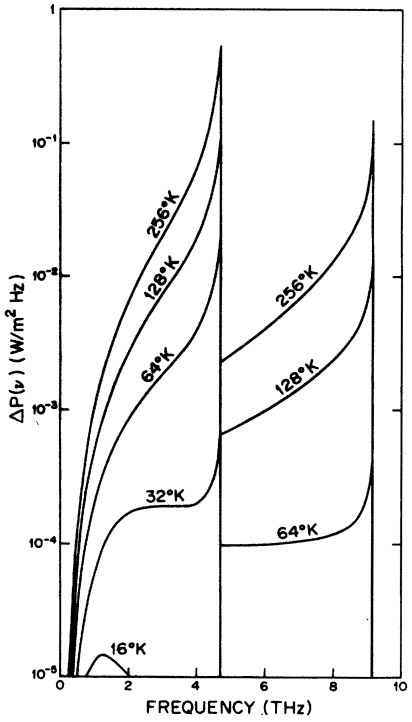

FIG. 8. Differential spectral energy flux at various temperatures as determined from the PB model. The discontinuities are at the cutoff frequency for transverse and longitudinal phonons in constantan treated as a Debye solid.

falls into the umklapp regime. The effect of umklapp processes is to increase the time high-frequency phonons spend in the heater film, i.e., to increase the escape time τ_b and thereby decrease the spectral flux below that expected in the absence of umklapp processes. It is worthwhile noting at this point that such umklapp processes are volume effects as distinct from interface effects.

The usual simplifying assumption that the transmission probability across the interface obtained from acoustic mismatch, i.e., e_σ is independent of frequency is, of course, only valid for phonon frequencies which are below the dispersive regions in *both* the heater *and* the transport medium. The dispersive regime is reached at different frequencies depending on crystal direction but should generally be at lower frequencies in SrF_2 than in constantan. From the dispersion relations found by Elcombe[23] we estimate that dispersion becomes significant beyond 2–3 THz. Quite severe mismatch may occur at frequencies and directions corresponding to zone boundaries. However, for any one phonon frequency the number of such directions should be of order small compared to those in a general propagation direction. The breakdown of the frequency independence of the acoustic mismatch almost certainly occurs and is a likely contributor to the effect observed in the present experiment.

Although it will not be possible to confirm the existence of T_e, it is at least possible to check if indeed the electron-electron interaction time in constantan is much shorter than the experimental observation time. We take the electrical resistivity of constantan at low temperatures to be limited by atomic disorder so that the electron-electron scattering time, τ_{ee}, can be adequately written in the Drude form

$$\tau_{ee} = \frac{m_e \sigma}{e^2 n}$$

in which m_e is the electron mass, e its charge, σ the electrical conductivity[8] equal to $\sim 1 \times 10^4\ \Omega^{-1}$ cm^{-1}, and n the electron concentration. We find for constantan a value of $\sim 1 \times 10^{-15}$ sec, which is some 10^7 times shorter than the observation time. This value must also be compared to the electron-phonon interaction time which is found[4] to be $0.03 < \tau_{ep} < 0.8$ nsec for the range of phonon frequencies of interest here.

We next turn our attention to Eq. (9) which is the form of the electron-phonon interaction used in the PB model. The origin of this form from the Pippard mechanism has been discussed by Ziman.[28] We limit the discussion here to whether or not the general criteria for the formulation of Eq. (9) are met. Among these is the requirement $q\lambda_e > 1$. The electron mean free path is $\lambda_e \equiv v_F \tau_{ee}$ and is, therefore, of order 10^{-7} cm, whereas q for 200 GHz phonons is of order 10^8 cm^{-1}. The condition is accordingly fulfilled for the lowest-frequency phonons of interest and is obviously fulfilled for yet higher-frequency phonons. The relation (9) has also been obtained for semiconductors by Bardeen and Shockley[29] from a quantum-mechanical treatment of the electron-phonon scattering matrix elements using a deformation potential approach. The relation is obtained only if the strain associated with the phonon varies slowly compared to interatomic distances. This may not be satisfied for phonons of frequency 3–6 THz for which we estimate q approaches nearly half the distance to the Brillouin zone boundary of constantan.

The limitations in the applicability of the deformation potential, the presence of umklapp processes, and frequency-dependent mismatch deserve further attention, as does the assumption that the electron-phonon transport in the heater film can be adequately described by simple rate processes. It is possible, therefore, that the currently extant models are insufficient to describe high-frequency phonon generation and transport, although there

exists neither experimental nor theoretical verification of this contention. In the absence of such verification, we turn instead to a phenomenological interpretation of the results.

B. Phenomenological filter

The experimental results shown in Figs. 5–7 clearly indicate that most of the phonon power transmitted through the film-crystal interface is carried by phonons of frequency $\lesssim 2.6$ THz, regardless of input power. This is in contradiction to both theoretical models which predict that as the input power increases an ever-increasing fraction of the power is carried by phonons of $\nu > 2.6$ THz. On a phenomenological basis, the contradiction can be resolved if there exists somewhere in the transport process a frequency-dependent reflective filter, which is a progressively poorer transmitter of phonons as the frequency increases. As a consequence, high-frequency phonons would spend longer periods of time in the heater film than is envisioned in both models, thereby building up the high-frequency phonon population in the film. The film becomes "hotter."

It is possible to extract the frequency dependence of the empirical filter, $F(\nu)$ from the experiment by noting that it must be the ratio of the experimentally observed spectral energy flux ΔP_{exp} to that which is incident on the interface in the presence of the filter, $P_I(\nu)$. The latter distribution we shall assume is given by the PB model except that the appropriate T_e is given by the energy balance between the input power and the phonon escape rate controlled by the frequency-dependent filter and not by e_a as in Eq. (8). As will be demonstrated shortly, the use of the PB spectral energy flux is itself a serious oversimplification because anharmonic decay of high-frequency phonons is neglected. Nevertheless, the $F(\nu)$ obtained neglecting phonon decay yields qualitative information on the frequency dependence of the filtering process. Accordingly, the function $F(\nu)$ has been determined numerically through an iteration of the expression

$$\Delta P_{\text{PB}}(T_e)F(\nu) = \Delta P_{\text{exp}}$$

until $F(\nu)$ no longer changes. To obtain $F(\nu)$ on an absolute scale we make the additional assumption that the value of $F(\nu = 0.2 \text{ THz})$ is the weighted average of the acoustic mismatch transmission coefficients e_l and e_t. This assumption is based on Wigmore's results[7] which show the AM model to be applicable up to $\nu = 0.29$ THz.

The results of the calculation are shown in Fig. 9. A marked decrease appears in the filter function between 0.2 and 2.6 THz with a further, even more marked, decrease above 2.6 THz. We conclude that the relaxation time τ_b for high-frequency phonons to cross the film-crystal interface is much longer than that predicted by acoustic mismatch. For example, the relaxation time obtained for 3-THz longitudinal phonons from Eq. (8) with $d = 6000$ Å,[30] $C_g = 5.24 \times 10^3$ m/sec, and $\eta_l = e_l^{-1} = 1.2$ yields $\tau_b = 5.6 \times 10^{-10}$ sec, whereas the value obtained by substituting $F(\nu = 3 \text{ THz})$ for η^{-1} is $\tau_b = 2.4 \times 10^{-7}$ sec. This time must be compared to the relaxation time for phonon decay. We assume that the dominant decay mode is $l \rightarrow l + t$ for which we obtain a relaxation time for 3-THz longitudinal phonons of $\sim 2 \times 10^{-10}$ sec by scaling the results of Orbach and Vredevoe.[31] It is likely, therefore, that before high-frequency phonons can escape the heater film they decay into lower-frequency phonons. The latter phonons can more easily escape into the crystal enriching, thereby, the low-frequency component of ΔP_{exp}. It is clear that anharmonic phonon decay must be included in a more complete treatment of the filtering process.

The empirical filter function $F(\nu)$ suggests another possible source in addition to the ones already mentioned. The sharp decrease in the function in the 1-THz range corresponds to a phonon wavelength of ~ 30 Å. It is possible that surface irregularities of such dimension appear at the

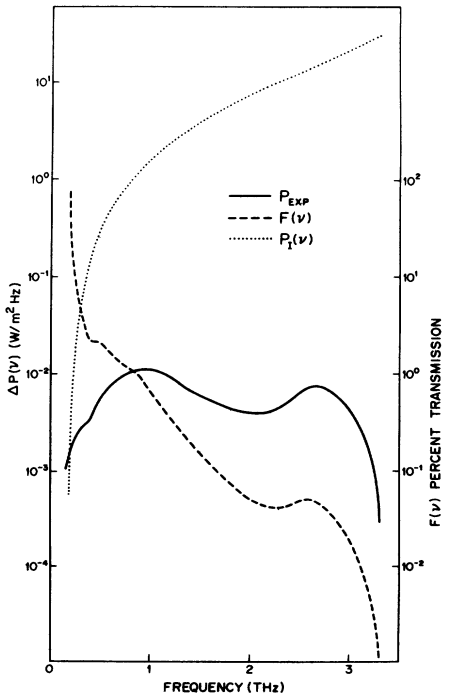

FIG. 9. Empirical filter function $F(\nu)$, compared to the experimental spectral energy flux P_{exp}, and the spectral energy flux incident on the interface P_I.

film-crystal interface to form strong scattering sites for short-wavelength phonons. The irregularities may be structural defects in either the metal film or in the SrF_2 surface or may be discontinuities in the bonding between the film and the crystal.[2]

The results of the experiment shed no further light as to which, if any, of the above mentioned sources is responsible for the filtering action. It is possible in future experiments to distinguish between volume and interface effects by repeating the experiment with films of different dimensions keeping constant the total input power per unit interface area. Similarly, it is possible to distinguish among the possible interface effects by varying surface conditions and film deposition methods.

C. Properties of phonon spectrometer

In the present experiment and in that presented in the following paper we describe the application of the vibronic sideband spectrometer to the study of the spectral, spatial, and temporal resolution of a heat pulse. The spectrometer is not limited to this application and is, in fact, applicable to a wide range of experiments. It is useful, therefore, to list its main characteristics.

Any crystal system which exhibits sharp zero-phonon spectral lines may be a suitable spectrometer. Such lines, with accompanying vibronic sidebands, have been reported in a literature too large to cite here. Suitable probes range from rare-earth ions to bound excitons, molecules and color centers. Any host material with a suitable energy gap is usable. References to observed vibronic structure in ionic crystals, covalent crystals, semiconductors, and glasses can be found in the literature. The specific parameters of the spectrometer will depend on the crystal system. We cite here those appropriate to $SrF_2:Eu^{2+}$. The spectral range is limited at low frequencies to 100–200 GHz by the width and displacement of the zero-phonon line, and at high frequencies by the phonon cutoff. The spectrometer can be scanned continuously and does not require an external electric or magnetic field for this purpose as does the recently proposed ruby spectrometer.[32] Spectral resolution is limited to ~100 GHz by the width of the zero-phonon line. Spatial resolution is determined by the diameter of the pump laser beam. We are able to obtain a diameter of 0.1 mm without much effort. Temporal resolution depends, in principle, only on the response time of the photomultiplier tube and the gate time of the signal recovery system. The combined limit of 1 nsec can be obtained with commercially available components. In practice, spectral and temporal resolution may be limited by the signal amplitude. Other methods than heater films may be used to generate phonons. For example, we have made observations on phonons produced by interaction of CO_2 and far-ir laser light with the SrF_2 crystal. The phonons need not be generated at the surface, but may be generated anywhere in the crystal as is the case of those mentioned in Sec. II, which are generated in the bulk through nonradiative decay.

VI. CONCLUSION

It has been demonstrated that existing theories of the spectral distribution of phonons emitted into a solid by Joule heating of thin films are insufficient to describe the experimental results for phonon frequencies above 1 THz. The discrepancy between theory and experiment is stated in terms of an empirical filtering action whose frequency dependence is determined from experiment in terms of limiting, simplifying assumptions. It has been further demonstrated that the vibronic sideband spectrometer developed during the course of this work, and described further in the following paper, offers unique potential for the study of high-frequency phonon transport.

ACKNOWLEDGMENTS

The authors acknowledge helpful discussions with R. Bray, R. Orbach, and W. L. Schaich.

---

*Work supported by NSF Grant Nos. 72-02070 and 76-23571. One of the authors (W.G.) acknowledges a travel grant from the Deutsche Forschungsgemeinschaft.

[1]See R. J. von Gutfeld, *Physical Acoustics*, edited by W. P. Mason (Academic, New York, 1968), Vol. 5.
[2]W. A. Little, Can. J. Phys. 37, 334 (1959).
[3]O. Weis, Z. Angew, Phys. 26, 325 (1969).
[4]H. J. Maris, J. Phys. (Paris) 33, C4-3 (1972).
[5]N. Perrin and H. Budd, Phys. Rev. Lett. 28, 1701 (1972); J. Phys. (Paris) 33, C4-33 (1972).
[6]J. Shah, R. F. Leheny, and A. H. Dayem, Phys. Rev. Lett. 33, 818 (1974).
[7]J. K. Wigmore, Phys. Rev. B 5, 700 (1972).
[8]P. Herth and O. Weis, Z. Angew. Phys. 29, 101 (1970).
[9]W. E. Bron and W. Grill, Phys. Rev. B 16, 5315 (1977) (following paper).
[10]Optovac, Inc., North Brookfield, Mass.
[11]L. L. Chase, Phys. Rev. B 2, 2308 (1970).
[12]D. E. McCumber and M. D. Sturge, J. Appl. Phys. 34, 1682 (1963).

[13]A similar technique has been used in Ref. 6.
[14]W. E. Bron, Phys. Rev. B 11, 3951 (1975).
[15]W. E. Bron and M. Wagner, Phys. Rev. 139, A233 (1965).
[16]W. E. Bron, Phys. Rev. 140, A2005 (1965); M. Wagner, Z. Phys. 214, 78 (1968).
[17]K. K. Rebane, *Impurity Spectra of Solids* (Plenum, New York, 1970); M. H. L. Pryce, *Phonons In Perfect Lattices and in Lattices with Point Imperfections*, edited by R. W. H. Stevenson (Oliver and Boyd, Edinburgh, 1966); G. Chioratti; *Theory of Imperfect Crystalline Solids* (Trieste Lectures) (International Atomic Energy Agency, Vienna, 1971).
[18]A. Man and W. E. Bron, Phys. Rev. B 13, 5591 (1976).
[19]L. E. Gurevich and T. M. Gasymov, Fiz. Tverd. Tela 9, 106 (1967) [Sov. Phys.-Solid State 9, 78 (1967)].
[20]A. B. Pippard, Philos. Mag. 46, 1104 (1955).
[21]J. A. Rayne and C. K. Jones, *Physical Acoustics*, edited by W. P. Mason and R. N. Thurston (Academic, New York, 1970), Vol. 7.
[22]Equation (12) is meant to be the sum of the integrant over each phonon branch.
[23]M. M. Elcombe, J. Phys. C 5, 2702 (1972).
[24]D. Gerlich, Phys. Rev. A 136, 1366 (1960).
[25]W. E. Bron and F. Keilmann, Phys. Rev. B 12, 2496 (1975).
[26]S. K. Sinha, Phys. Rev. 143, 422 (1966).
[27]R. J. Birgeneau, J. Cordes, G. Dolling, and A. D. B. Woods, Phys. Rev. 136, A1359 (1964).
[28]J. M. Ziman, *Electrons and Phonons* (Clarendon, Oxford, 1960).
[29]J. Bardeen and W. Shockley, Phys. Rev. 77, 407 (1950); Phys. Rev. 80, 72 (1950).
[30]In the presence of strong reflection at the interface we take the effective dimension of the film to be twice its thickness in order to take into account phonons with originally negative wave vectors.
[31]R. Orbach and L. A. Vredevoe, Physics (N.Y.) 1, 91 (1964).
[32]R. S. Meltzer and J. E. Rives, Phys. Rev. Lett. 8, 421 (1977).